Load reduction of a monopile wind turbine tower using optimal tuned mass dampers

Xin Tong[a], Xiaowei Zhao[a] * and Shi Zhao[b]

[a] *School of Engineering, University of Warwick, Coventry, CV4 7AL, UK*; [b] *Department of Engineering Science, University of Oxford, Parks Road, Oxford, OX1 3PJ, UK*

We investigate to apply tuned mass dampers (TMDs) (one in the fore-aft direction, one in the side-side direction) to suppress the vibration of a monopile wind turbine tower. Using the spectral element method, we derive a finite-dimensional state space model Σ_d from an infinite-dimensional model Σ of a monopile wind turbine tower stabilized by a TMD located in the nacelle. Σ and Σ_d can be used to represent the dynamics of the tower and TMD in either the fore-aft direction or the side-side direction. The wind turbine tower subsystem of Σ is modelled as a non-uniform SCOLE (NASA Spacecraft Control Laboratory Experiment) system consisting of an Euler-Bernoulli beam equation describing the dynamics of the flexible tower and the Newton-Euler rigid body equations describing the dynamics of the heavy rotor-nacelle assembly (RNA) by neglecting any coupling with blade motions. Σ_d can be used for fast & accurate simulation for the dynamics of the wind turbine tower as well as for optimal TMD designs. We show that Σ_d agrees very well with the FAST (Fatigue, Aerodynamics, Structures, and Turbulence) simulation of the NREL 5-MW wind turbine model. We optimize the parameters of the TMD by minimizing the frequency-limited $\mathcal{H}_2$-norm of the transfer function matrix of Σ_d which has input of force and torque acting on the RNA, and output of tower-top displacement. The performances of the optimal TMDs in the fore-aft and side-side directions are tested through FAST simulations, which achieve substantial fatigue load reductions. This research also demonstrates how to optimally tune TMDs to reduce vibrations of flexible structures described by partial differential equations.

Keywords: monopile wind turbine tower; SCOLE model; tuned mass damper; spectral element method; frequency-limited $\mathcal{H}_2$-norm; FAST code

1. Introduction

Wind power has become an important source of green energy with continued substantial increases in investments. The proportion of global wind power capacity in the total energy generation capacity is expected to increase to 9.1% by 2020 (see BTM Consult, 2011) from about 2.5% in 2010 (see World Wind Energy Association [WWEA], 2011). To capture higher-quality wind resource, large wind turbines are being further constructed offshore. For example offshore wind power contributed 14.04% of total wind power capacity installed in Europe in 2013 (see The European Wind Energy Association [EWEA], 2014), and the European offshore wind power capacity is expected to increase to 40 GW, accounting for 4% of the European Union's electrical demand, by 2020 (see Teena, 2010). However, due to severe weather, turbulence and wave conditions, offshore wind turbines bear significant fluctuating loads and vibrations leading to structural fatigue. Therefore, it is of critical importance to develop control techniques to reduce vibration loads acting on the wind turbine towers to increase their life expectancy and enable the construction of lighter and cheaper wind turbine towers. Nowadays, offshore wind turbines are principally fixed-bottom substructures. Most of fixed-bottom offshore turbines are monopiles (see Stewart & Lackner, 2013), which is the type investigated in this paper. We call this monopile-tower assembly as the monopile wind turbine

*Corresponding author. Email:xiaowei.zhao@warwick.ac.uk

tower.

1.1 *Active control of wind turbine towers*

A lot of research has proposed approaches to mitigate loads on the wind turbine towers. The conventional method is the blade pitch control. Leithead, Dominguez, and Spruce (2004) tuned the blade pitch angles based on the measurement of tower accelerations to cancel the tower fore-aft mode. Darrow (2010) added a new tower velocity feedback loop into the CART3 (Controls Advanced Research Turbine) baseline collective pitch control loop to damp the tower fore-aft motion. Soltani, Wisniewski, Brath, and Boyd (2011) employed receding horizon control to calculate the optimal collective pitch angles based on the estimated mean wind speed from LiDAR (Light Detection and Ranging), which reduced structural loads and power fluctuations significantly. However blade pitch control is effective at the expense of interfering with power generation and increasing blade pitch actuator usage (thus leading to fatigue). Zhao and Weiss (2011a, 2014) and Zhang, Neilsen, Blaabjerg, and Zhou (2014) proposed to suppress the side-side vibration of the wind turbine towers by modulating the generator torque. But this type of control action is likely to interfere with the proper functioning of the wind turbines.

1.2 *Passive structural control of wind turbine towers*

Structural control, which is initially used in civil engineering to protect structures from dynamic loadings due to earthquakes, stout winds, waves and other sources (see Soong & Spencer, 2002), might offer a good alternative solution. There are three major categories of structural control methods - passive, semi-active and active control (see Spencer & Nagarajaiah, 2003). Passive structural control, such as tuned mass damper (TMD), is the simplest among these three approaches since its controller has constant parameters. TMD consists of a large mass, springs and dampers, among which the mass is linked to the structure to be stabilized via the springs and the dampers. The mechanism is that the TMD is tuned to a particular structural frequency and thus will resonate and dissipate input energy via the dampers when the structure is excited at that particular frequency. TMDs have been successfully used in the vibration reduction of tall buildings such as the John Hancock Tower in Boston and the Citicorp Center in Manhattan (see Sadek, Mohraz, Taylor, & Chung, 1997), which can normally decrease the worst-case wind-induced motion of the building by about 50%.

1.2.1 Previous work

Lackner and Rotea (2011) added structural control capacity to the famous wind turbine simulation code FAST (Fatigue, Aerodynamics, Structures, and Turbulence) by incorporating two independent TMDs into the nacelle which translate in the side-side and fore-aft directions, as shown in Figure 1. This modified version of FAST is called FAST-SC. The NREL (National Renewable Energy Laboratory) 5-MW wind turbine model was used for simulation. A brief introduction on the NREL 5-MW baseline wind turbine model and the FAST will be given in Section 2. Lackner and Rotea (2011) chose an optimal passive TMD in the fore-aft direction to reduce structural loads acting on the wind turbine tower with only the first tower fore-aft bending mode being considered. The mass of the TMD was set to be about 2% of the total turbine mass. The spring constant of the TMD was chosen such that the natural frequency of the TMD equaled the first fore-aft modal frequency of the tower. The damping constant was determined by trial and error to minimize the standard deviation of tower-top fore-aft translational deflections. The results commentated the effectiveness of TMD in improving the wind turbine tower's structural response.

Stewart and Lackner (2013) advanced the results in Lackner and Rotea (2011) with the similar TMD setup but more advanced optimizing method based on limited DOF control design models (for four types of turbine platforms), which were obtained by only considering the specific degrees

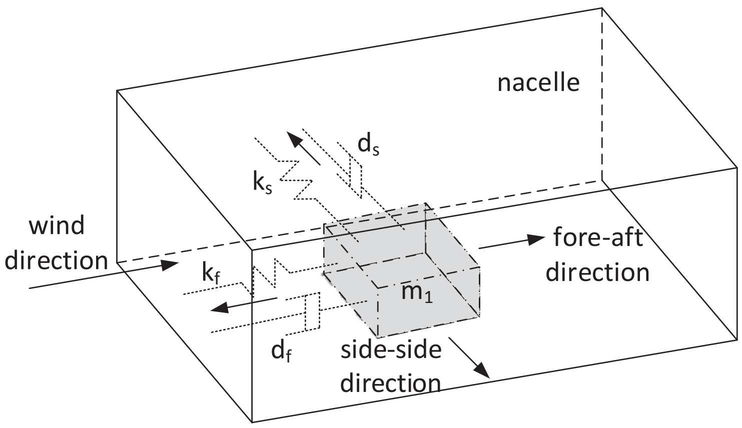

Figure 1. Configuration of fore-aft and side-side TMDs in a nacelle showing their moving directions. Both TMDs share the same mass component m_1 but have different spring and damping constants (k_f vs k_s and d_f vs d_s). While this is not shown in the figure, the mass component can be either put on the floor of the nacelle through wheels/racks like the cases of John Hancock Tower in Boston and the Citicorp Center in Manhattan, or hanged above the floor through cables like the case of Taipei 101 skyscraper in Taipei.

of freedom that contributed most of the loading. In this paper we only consider the monopile wind turbine tower, for which the limited DOF model in Stewart and Lackner (2013) was a TMD-stabilized rigid inverted pendulum with the base stiffness and damping modelled as rotational spring and damper. The spring and damping constants of the rigid inverted pendulum were obtained through a non-linear least square algorithm based on a FAST-SC simulation. Then the optimization of the spring and damping constants of the TMD was through dynamic simulations of the TMD-stabilized rigid inverted pendulum under a specific exciting loading with different combinations of spring and damping constants of the TMD. The optimal TMD was the one which minimized the standard deviation of the displacement of the top of the inverted pendulum (which denotes the top of the wind turbine tower). The exciting loading was a combination of a deflection step input, and a constant thrust moment which was obtained through FAST-SC simulation at rated wind speed. Finally they conducted a simulation in the FAST-SC using the optimal TMD, which showed substantial fatigue load reduction.

We did a simulation for the fore-aft and side-side deflections of the NREL 5-MW monopile wind turbine tower at a certain time instant using FAST, which was shown in Figure 2, from which one can see clearly that the wind turbine tower is not a rigid inverted pendulum as in Stewart and Lackner (2013) but a flexible beam. Because the first tower bending mode dominates the

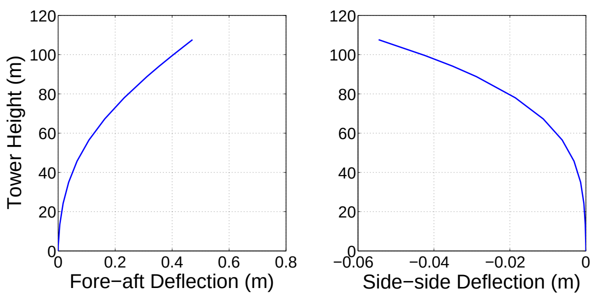

Figure 2. Deflections of the NREL 5-MW monopile wind turbine tower at a certain time instant by FAST simulation.

dynamic response of a typical monopile wind turbine tower subject to wind and wave loads (see Lackner & Rotea, 2011), and the largest deflection for this first mode occurs at the tower top as shown in Figure 2 of this paper and Figure 10 of J. Jonkman, Marshall, and Buhl (2005), it is acceptable to use an inverted pendulum as control design model to only control the first mode. But apparently the inverted pendulum cannot be used to simulate the dynamics of the wind turbine tower. Stewart and Lackner (2013) mentioned that desirably the parameter optimization of the TMD should be based on the FAST-SC simulation which was unfortunately an overkill because a 10-min simulation time approximately took a computation of 10-30 minutes. So a rigid rod in Stewart and Lackner (2013) was used to model the turbine tower (with a big mass at its top as the heavy rotor-nacelle assembly (RNA)) because fortunately there was usually only one degree of freedom accounting for most fatigue load for the types of wind turbine towers considered in Stewart and Lackner (2013). But a rigid rod might not be able to model other types of wind turbine towers or more generally other flexible beams (which have more modes dominating the vibrations) even only for control design purpose. Thus it is more sensible to use a type of beam equations to model the wind turbine tower, which can be used to conduct both control design and fast & accurate simulation, whose TMD design method should also be easily extended to other types of flexible structures. In addition, in Stewart and Lackner (2013) the parameters of the inverted pendulum had to be obtained through identification procedure from the NREL 5-MW monopile wind turbine model using FAST simulation under a step input of the tower deflection without wind or wave loading applied. In practice this kind of identification will be very difficult to conduct on a real wind turbine. Desirably the parameters of the control design model should be obtained directly or through simple computations from the tower specifications provided by the manufacturers. Furthermore, the optimization of the TMD system in Stewart and Lackner (2013) was conducted based on a specific loading excitation obtained from FAST-SC simulation. It will be nice to have a proper mathematical formulation and systematic design method for the optimization procedure, which can take account of more general wind and wave excitations and can be extended to the vibration control of other types of flexible structures.

1.2.2 Modelling, simulation and optimal TMD design of a monopile wind turbine tower based on the SCOLE beam system and H_2 optimization

Zhao and Weiss (2011a, 2011b) used a non-uniform NASA SCOLE (Spacecraft Control Laboratory Experiment) system to model the monopile wind turbine tower in either the fore-aft plane or the side-side plane. The SCOLE system is a well known model for a flexible beam with one end clamped and the other end connected to a rigid body. Originally it has been developed to model a flexible mast carrying an antenna on a satellite (see Littman & Markus, 1988a, 1988b). For more details about the SCOLE model, we refer to these four papers which contain many references for previous work (controllability, observability, stabilization by static feedback etc) in the framework of infinite-dimensional systems which are systems described by partial differential equations (PDEs). As you will see in Section 3.1, the flexible beam in the SCOLE model is described by a PDE. This SCOLE system is very suitable to model the monopile wind turbine tower, which has the bottom end clamped in the ocean floor and the upper end linked to the RNA.

Zhao and Weiss (2015) incorporated a TMD into the SCOLE model denoted by Σ, and showed its strong stability. The mass component of the TMD can be either put on the floor of the nacelle through wheels/racks (reducing friction) or hanged above the floor through cables. In the present paper we discretize this infinite-dimensional SCOLE-TMD system Σ into a finite-dimensional model Σ_d using the spectral element method and then verify Σ_d against the FAST-SC simulation of the NREL 5-MW wind turbine model. Σ_d is able to describe the dynamics of the tower and TMD in either the fore-aft direction or the side-side direction with corresponding parameter choices. Finally we derive the fore-aft and side-side optimal TMDs by minimizing the $\mathcal{H}_2$-norm of Σ_d with external force and torque as input and the tower-top displacement as output, which means to minimize the standard deviation of the tower-top displacement under external excitation. We get similar vibration suppression performance as Stewart and Lackner (2013). But our model and optimization method satisfy all the desirable improvements mentioned in Section 1.2.1. More generally, our paper also demonstrates how to optimally tune TMDs to reduce vibrations of flexible structures described by PDEs.

1.3 *Structure of the paper*

The structure of the paper is as follows. In Section 2, we introduce our simulation environment of the NREL 5-MW baseline monopile wind turbine model within the FAST code and its modified version FAST-SC which accommodated structural control. First, we introduce the structure of the FAST simulation code consisting of FAST, AeroDyn, HydroDyn, and MATLAB/Simulink® interface through which one can simulate the wind turbine dynamics. Then we introduce FAST-SC. Finally, we talk about the NREL 5-MW baseline wind turbine model. In Section 3, we introduce the infinite-dimensional model of a monopile wind turbine tower stabilized by a TMD system located in the nacelle, denoted by Σ. We then reformulate it to state space format. Subsequently we discretize Σ along the tower span using the spectral element method to derive its finite-dimensional version Σ_d. Finally we verify Σ_d against the FAST/FAST-SC simulation of the NREL 5-MW wind turbine model. In Section 4, we conduct optimal design for the TMDs based on Σ_d. The spring and damping constants of the TMD are the design parameters with a fixed mass component being 2% of the total structural mass of the turbine. The design parameters are obtained by minimizing the $\mathcal{H}_2$-norm of the transfer function matrix of Σ_d with force and torque input and tower-top displacement output. Here we use the frequency-limited version of the $\mathcal{H}_2$-norm which means to compute the $\mathcal{H}_2$-norm over a small interval around the first modal frequency of the monopile wind turbine tower. Finally, an optimal fore-aft TMD and an optimal side-side TMD are obtained. In Section 5, we carry out simulations using the NREL 5-MW monopile wind turbine model within FAST/FAST-SC to test the effectiveness of our optimal TMDs. Section 6 concludes this paper.

2. Introduction to the NREL 5-MW baseline monopile wind turbine model within FAST simulation environment

In this section we briefly introduce our simulation platform – the NREL 5-MW baseline monopile wind turbine model within FAST simulation environment as shown in Figure 3. The FAST code written by NREL models the wind turbine comprising rigid and flexible bodies coupled using several degrees of freedom (DOFs). There are four DOFs accounting for tower bending – two originating from the fore-aft modes and two from the side-side modes.

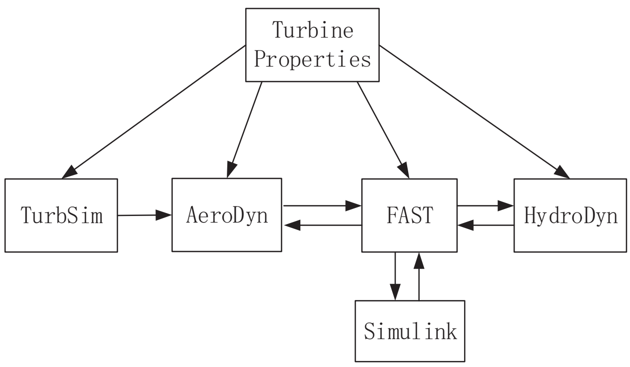

Figure 3. Block diagram of the structure of the NREL FAST simulation environment.

AeroDyn is a subroutine, developed by NREL, to compute aerodynamic forces along the blades, which are used to solve equations of motion in FAST. AeroDyn requires instant turbine information obtained from FAST to model aerodynamics (see NWTC, 2014a). Full-field turbulence required by AeroDyn can be created by TurbSim, whose details can be found in NWTC (2014b). HydroDyn is coupled to FAST for the aero-hydro-servo-elastic simulations of offshore wind turbines. It receives the position, orientation, velocities, and accelerations of the substructure from FAST at each coupling time step and then calculates hydrodynamic loads and sends them back to FAST (see J. M. Jonkman, Robertson, & Hayman, to appear). The FAST subroutines have been linked with a MATLAB standard gateway subroutine so that Matlab/Simulink is able to encapsulate FAST's structural dynamic routines, AeroDyn's aerodynamic routines, HydroDyn's hydrodynamic routines, and the interfaces to MATLAB/Simulink into an S-Function block (see J. Jonkman et al., 2005). This feature enables flexible control design of the wind turbine in the Simulink environment.

To equip FAST code with structural control, Lackner and Rotea (2011) developed FAST-SC. It includes two independent TMDs located in the nacelle, one in the fore-aft direction and the other in the side-side direction, as shown in Figure 1. The NREL offshore 5-MW baseline wind turbine model represents the current typical offshore turbines, whose properties are given in J. Jonkman (2006). The model has three operation regions with the cut-in wind speed of 3 m/s, rated wind speed of 11.4 m/s, and cut-out wind speed of 25 m/s. More information can be found in J. Jonkman, Butterfield, Musial, and Scott (2009).

3. System modelling

3.1 *An infinite-dimensional model of the monopile wind turbine tower stabilized by a TMD located in the nacelle*

The SCOLE system is a well known model for a flexible beam with one end clamped and the other end connected to a rigid body. Like in Zhao and Weiss (2011a, 2011b), here we use it to model a monopile wind turbine tower that has the bottom end clamped in the ocean floor and the upper end linked to the heavy rigid RNA by neglecting any coupling with blade motions. We mention that the SCOLE system can be used to represent the tower dynamics in the fore-aft plane and in the side-side plane respectively with corresponding parameter choices. In this paper, we design a TMD in each plane respectively to reduce vibration loads of the whole monopile wind turbine tower because all vibrations can be decomposed into these two orthogonal planes. The two TMDs share the same mass component, but have different springs and dampers as shown in Figure 1. The spring and damper components of the TMD system in each plane connect at one end to the nacelle and link at the other end to its mass component in parallel. The mass component of the TMD is put on the floor of the nacelle through wheels/racks or hanged above the floor through cables. The mathematical model Σ of the monopile wind turbine tower stabilized by a TMD, in either the fore-aft plane or the side-side plane, is shown below (see Zhao & Weiss, 2015).

$$\begin{cases} \rho(x)w_{tt}(x,t) + (EI(x)w_{xx}(x,t))_{xx} = 0, \quad (x,t) \in (0,l) \times [0,\infty), & (3.1) \\ w(0,t) = 0, \; w_x(0,t) = 0, & (3.2) \\ mw_{tt}(l,t) - (EIw_{xx})_x(l,t) = F_e(t) + k_1(p(t) - w(l,t)) + d_1(p_t(t) - w_t(l,t)), & (3.3) \\ Jw_{xtt}(l,t) + EI(l)w_{xx}(l,t) = T_e(t), & (3.4) \\ m_1 p_{tt}(t) = k_1(w(l,t) - p(t)) + d_1(w_t(l,t) - p_t(t)), & (3.5) \end{cases}$$

where the subscripts t and x denote derivatives with respect to the time t and the position x. The equations (3.1)-(3.4) are the non-uniform monopile wind turbine tower subsystem while the equation (3.5) is the TMD subsystem. We introduce the tower subsystem (3.1)-(3.4) first. (3.1) is Euler-Bernoulli beam equation which represents the dynamics of the flexible tower while (3.2) means that the tower is clamped. (3.3)-(3.4) are the Newton-Euler rigid body equations which represent the dynamics of the RNA. l, ρ and EI denote the tower's height, mass density function and flexural rigidity function while w denotes the translational displacement of the tower. $\rho, EI \in C^4[0,l]$ are assumed to be strictly positive functions. The parameters $m > 0$ and $J > 0$ are the mass and the moment of inertia of the RNA. F_e and T_e denote the aerodynamic force and the aerodynamic torque acting on the RNA. In the TMD system (3.5), $m_1 > 0$, $k_1 > 0$ and $d_1 > 0$ are the mass, spring constant and damping coefficient of the TMD. Both subsystems are interconnected through the translational velocity of the RNA (tower-top translational velocity) $w_t(l,t)$ and the force $(k_1(p(t) - w(l,t)) + d_1(p_t(t) - w_t(l,t)))$ generated by the TMD system.

The state of Σ at the time t is

$$z(t) = \begin{bmatrix} z_1(t) \\ z_2(t) \\ z_3(t) \\ z_4(t) \\ z_5(t) \\ z_6(t) \end{bmatrix} = \begin{bmatrix} w(\cdot,t) \\ w_t(\cdot,t) \\ w_t(l,t) \\ w_{xt}(l,t) \\ p(t) - w(l,t) \\ p_t(t) \end{bmatrix}, \tag{3.6}$$

where z_1 and z_2 are the translational displacement and velocity of the tower. z_3 and z_4 are the translational velocity and angular velocity of the nacelle. z_5 and z_6 are the position and translational velocity of the mass component of the TMD. The natural energy state space of Σ is

$$X = \mathcal{H}_l^2(0,l) \times L^2[0,l] \times \mathbb{C}^4, \tag{3.7}$$

where

$$\mathcal{H}_l^2(0,l) = \{h \in \mathcal{H}^2(0,l) \mid h(0) = 0,\ h_x(0) = 0\}. \tag{3.8}$$

Here $\mathcal{H}^n$ ($n \in \mathbb{N}$) denotes the usual Sobolev spaces. Zhao and Weiss (2015) proved that Σ is strongly stable on X.

3.2 *Discretizing the TMD-stabilized monopile wind turbine tower model* $\boldsymbol{\Sigma}$

In this section we use the spectral element method to discretize the infinite-dimensional TMD-stabilized monopile wind turbine tower model Σ (3.1)-(3.5) in spatial domain to achieve our purpose for fast simulation and TMD optimization. For this purpose, we normalize the spatial domain $x \in (0,l)$ of Σ to the standard domain $x \in (-1,1)$.

The first step is to obtain the weak form of the governing equation. Multiplying both sides of the equation (3.1) with a weight function $u(x)$ and integrating over the domain $x \in (-1,1)$ yield

$$\int_{-1}^{1} \{\rho w_{tt} u + (EI w_{xx})_{xx} u\} \mathrm{d}x = 0. \tag{3.9}$$

Using integration by parts, we have

$$\int_{-1}^{1} \{\rho w_{tt} u + EI w_{xx} u_{xx}\} \mathrm{d}x + [(EI w_{xx})_x u - EI w_{xx} u_x]_{x=-1}^{x=1} = 0. \tag{3.10}$$

As in the finite element method, the weight function here is required to satisfy the essential boundary conditions (3.2), that is

$$u(x=-1) = u_x(x=-1) = 0. \tag{3.11}$$

Substituting equations (3.3)-(3.4) and (3.11) into (3.10), we get the weak form

$$\int_{-1}^{1}\{\rho w_{tt}u + EIw_{xx}u_{xx}\}\mathrm{d}x = \left[-mw_{tt} + F_e + k_1(p-w) + d_1(p_t - w_t)\right]u\big|_{x=1} + \left(T_e - Jw_{xtt}\right)u_x\big|_{x=1}. \tag{3.12}$$

Moving all the terms containing time derivatives to the left-hand side of the equation and all other terms to the right-hand side, we have

$$\int_{-1}^{1}\{\rho w_{tt}u\}\mathrm{d}x + \left[mw_{tt}u - d_1(p_t - w_t)u\right]_{x=1} + \left[Jw_{xtt}u_x\right]_{x=1} = -\int_{-1}^{1}\{EIw_{xx}u_{xx}\}\mathrm{d}x + \left[F_e u + k_1(p-w)u\right]_{x=1} + T_e u_x\big|_{x=1}. \tag{3.13}$$

Now we introduce two new variables

$$v(x,t) = w_t(x,t), \tag{3.14}$$

and

$$r(t) = p_t(t) \tag{3.15}$$

which represents the translational velocity of the mass component of the TMD. Then equation (3.13) can be written as

$$\int_{-1}^{1}\{\rho v_t u\}\mathrm{d}x + \left[mv_t u - d_1(r - v)u\right]_{x=1} + \left[Jv_{xt}u_x\right]_{x=1} = -\int_{-1}^{1}\{EIw_{xx}u_{xx}\}\mathrm{d}x + \left[F_e u + k_1(p-w)u\right]_{x=1} + T_e u_x\big|_{x=1}. \tag{3.16}$$

The second step is to approximate the solution using high-order basis functions. Specifically, $w(x,t)$ is approximated by

$$w(x,t) = \sum_{n=0}^{N}\hat{w}_n(t)\psi_n(x), \tag{3.17}$$

where the basis function $\psi_n(x)$ needs to satisfy the essential boundary conditions

$$\psi_n(x=-1) = \frac{\mathrm{d}\psi_n}{\mathrm{d}x}(x=-1) = 0. \tag{3.18}$$

A convenient choice is

$$\psi_n(x) = (1+x)^2 T_n(x) \tag{3.19}$$

where $T_n(x)$ is the n_{th} Chebyshev polynomial (see Boyd, 2001).

Similarly,

$$v(x,t) = \sum_{n=0}^{N}\hat{v}_n(t)\psi_n(x) \tag{3.20}$$

and it is obvious that

$$\hat{v}_n = \frac{\mathrm{d}\hat{w}_n}{\mathrm{d}t} \quad \forall\, n \in \{0, 1, \cdots, N\}\,. \tag{3.21}$$

Substitute (3.20) for $v(x,t)$, (3.17) for $w(x,t)$ and $\psi_n(x)$ for $u(x)$ into (3.16) for $n \in \{0, 1, \cdots, N\}$. The resulting $N+1$ linear equations can be written in matrix form

$$\mathbf{E}\dot{\hat{\mathbf{v}}} = \mathbf{A_{21}}\hat{\mathbf{w}} + \mathbf{A_{22}}\hat{\mathbf{v}} + \mathbf{A_{23}}p + \mathbf{A_{24}}r + \mathbf{B_{21}}F_e + \mathbf{B_{22}}T_e \tag{3.22}$$

where

$$\hat{\mathbf{w}} = [\hat{w}_0, \hat{w}_1, \cdots, \hat{w}_N]^T \tag{3.23}$$

$$\hat{\mathbf{v}} = [\hat{v}_0, \hat{v}_1, \cdots, \hat{v}_N]^T \tag{3.24}$$

and each element of the matrices is given by

$$\mathbf{E}(i,j) = \int_{-1}^{1} \rho\psi_i\psi_j \mathrm{d}x + \left[m\psi_i\psi_j + J\frac{\mathrm{d}\psi_i}{\mathrm{d}x}\frac{\mathrm{d}\psi_j}{\mathrm{d}x}\right]_{x=1} \tag{3.25}$$

$$\mathbf{A_{21}}(i,j) = -\int_{-1}^{1} EI\frac{\mathrm{d}^2\psi_i}{\mathrm{d}x^2}\frac{\mathrm{d}^2\psi_j}{\mathrm{d}x^2}\mathrm{d}x - [k_1\psi_i\psi_j]_{x=1} \tag{3.26}$$

$$\mathbf{A_{22}}(i,j) = -[d_1\psi_i\psi_j]_{x=1} \tag{3.27}$$

$$\mathbf{A_{23}}(i) = k_1\psi_i|_{x=1} \tag{3.28}$$

$$\mathbf{A_{24}}(i) = d_1\psi_i|_{x=1} \tag{3.29}$$

$$\mathbf{B_{21}}(i) = \psi_i|_{x=1} \tag{3.30}$$

$$\mathbf{B_{22}}(i) = \left.\frac{\mathrm{d}\psi_i}{\mathrm{d}x}\right|_{x=1}. \tag{3.31}$$

Note that $\mathbf{E}, \mathbf{A_{21}}, \mathbf{A_{22}} \in \mathbb{R}^{(N+1)\times(N+1)}$ and $\mathbf{A_{23}}, \mathbf{A_{24}}, \mathbf{B_{21}}, \mathbf{B_{22}} \in \mathbb{R}^{(N+1)\times 1}$.

Equation (3.5) can be written as

$$m_1 r_t(t) = k_1(w(1,t) - p(t)) + d_1(v(1,t) - r(t)). \tag{3.32}$$

Substituting (3.20) for $v(x,t)$ and (3.17) for $w(x,t)$ into (3.32), we get

$$m_1 r_t = \mathbf{A_{41}}\hat{\mathbf{w}} + \mathbf{A_{42}}\hat{\mathbf{v}} - k_1 p - d_1 r \tag{3.33}$$

where $\mathbf{A_{41}}, \mathbf{A_{42}} \in \mathbb{R}^{1\times(N+1)}$ and

$$\mathbf{A_{41}}(j) = k_1\psi_j|_{x=1}, \tag{3.34}$$

$$\mathbf{A_{42}}(j) = d_1\psi_j|_{x=1}. \tag{3.35}$$

By the relations (3.15) and (3.21), the finite-dimensional model can be formulated as

$$\mathbf{M_1}\begin{bmatrix}\dot{\hat{\mathbf{w}}}\\ \dot{\hat{\mathbf{v}}}\\ \dot{p}\\ \dot{r}\end{bmatrix} = \mathbf{M_2}\begin{bmatrix}\hat{\mathbf{w}}\\ \hat{\mathbf{v}}\\ p\\ r\end{bmatrix} + \mathbf{M_3}\begin{bmatrix}F_e\\ T_e\end{bmatrix} \tag{3.36}$$

where

$$\mathbf{M_1} = \begin{bmatrix} \mathbf{I} & \mathbf{0} & \mathbf{0} & \mathbf{0} \\ \mathbf{0} & \mathbf{E} & \mathbf{0} & \mathbf{0} \\ \mathbf{0} & \mathbf{0} & 1 & 0 \\ \mathbf{0} & \mathbf{0} & 0 & m_1 \end{bmatrix}, \tag{3.37}$$

$$\mathbf{M_2} = \begin{bmatrix} \mathbf{0} & \mathbf{I} & \mathbf{0} & \mathbf{0} \\ \mathbf{A_{21}} & \mathbf{A_{22}} & \mathbf{A_{23}} & \mathbf{A_{24}} \\ \mathbf{0} & \mathbf{0} & 0 & 1 \\ \mathbf{A_{41}} & \mathbf{A_{42}} & -k_1 & -d_1 \end{bmatrix}, \tag{3.38}$$

$$\mathbf{M_3} = \begin{bmatrix} \mathbf{0} & \mathbf{0} \\ \mathbf{B_{21}} & \mathbf{B_{22}} \\ 0 & 0 \\ 0 & 0 \end{bmatrix} \tag{3.39}$$

and $\mathbf{I}$ is the identity matrix of appropriate size.

Note that the states $\hat{\mathbf{w}}$ and $\hat{\mathbf{v}}$ are spectral coefficients, rather than the values of $w(x,t)$ and $v(x,t)$ in the physical space. Thus we need to transform between the spectral space and the physical space. For example, to simulate tower movements and derive the tower deflection $w(x,t)$, we need to specify the initial conditions first. Suppose we have the initial conditions $w(x,0)$ and $v(x,0)$, we cannot assign these values to the ODE solver directly. Instead, we need to calculate the corresponding $\hat{\mathbf{w}}(0)$ and $\hat{\mathbf{v}}(0)$. It follows from (3.17) that

$$\begin{bmatrix} w(x_0,0) \\ \vdots \\ w(x_N,0) \end{bmatrix} = \mathbf{T}\hat{\mathbf{w}}(0) \tag{3.40}$$

where the matrix $\mathbf{T} \in \mathbb{R}^{(N+1)\times(N+1)}$ is given by

$$\mathbf{T}(i,j) = \psi_j|_{x=x_i} \tag{3.41}$$

and $x_i, i = 0, 1, \ldots, N$ are the collocation points

$$x_i = \begin{cases} \cos(\frac{i\pi}{N}), & i = 0, 1, \ldots, N-1 \\ \cos(\frac{(N-0.5)\pi}{N}), & i = N \end{cases}. \tag{3.42}$$

Note that the last collocation point is $x_N = \cos(\frac{(N-0.5)\pi}{N})$ instead of $x_N = \cos\pi = -1$. That is because $\psi_j(x=-1) = 0$ (see equation (3.18)), the last row of $\mathbf{T}$ would be a zero vector if $x_N = -1$. Such a $\mathbf{T}$ is guaranteed to be nonsingular. Now it is evident that

$$\hat{\mathbf{w}}(0) = \mathbf{T}^{-1} \begin{bmatrix} w(x_0,0) \\ \vdots \\ w(x_N,0) \end{bmatrix} \tag{3.43}$$

and $\hat{\mathbf{v}}(0)$ can be obtained in the same manner.

With the initial conditions, the model can be simulated easily, whose outputs $\hat{\mathbf{w}}(t)$ and $\hat{\mathbf{v}}(t)$ can be transformed to physical domain variables

$$\mathbf{w}(x,t) = \mathbf{T}\hat{\mathbf{w}}(t), \tag{3.44}$$

$$\mathbf{v}(x,t) = \mathbf{T}\hat{\mathbf{v}}(t), \tag{3.45}$$

where

$$\mathbf{w}(x,t) = [w(x_0,t), \dots, w(x_N,t)]^T, \tag{3.46}$$

$$\mathbf{v}(x,t) = [v(x_0,t), \dots, v(x_N,t)]^T. \tag{3.47}$$

Thus the state space formulation of the spatially discretized monopile wind turbine tower - TMD system Σ_d is

$$\begin{cases} \dot{\mathbf{X}} = \mathbf{A}\mathbf{X} + \mathbf{B}\mathbf{u} & (3.48) \\ \mathbf{Y} = \mathbf{C}\mathbf{X} & (3.49) \end{cases}$$

where the state $\mathbf{X} = [\hat{\mathbf{w}}, \hat{\mathbf{v}}, p, r]^T$, input $\mathbf{u} = [F_e, T_e]^T$, state matrix $\mathbf{A} = \mathbf{M_1}^{-1}\mathbf{M_2}$, input matrix $\mathbf{B} = \mathbf{M_1}^{-1}\mathbf{M_3}$. If $\mathbf{Y} = \mathbf{w}(x,t)$ (the whole tower deflection), output matrix $\mathbf{C} = [\mathbf{T}\ \mathbf{0}\ 0\ 0]$ while if $\mathbf{Y} = w(l,t)$ (tower-top translational displacement), $\mathbf{C} = [\mathbf{T}(\mathbf{1},:)\ \mathbf{0}\ 0\ 0]$. Based on Σ_d, we are not only able to conduct TMD designs using $\mathcal{H}_2$ optimization, but also able to simulate the tower dynamics (for example using the MATLAB built-in function *lsim*).

3.3 *Model verification*

We now verify our monopile wind turbine tower model Σ_d (3.48) - (3.49) against the NREL 5-MW monopile wind turbine tower model within FAST/FAST-SC simulation. Σ_d can be used to represent the dynamics of the tower and TMD in the fore-aft direction and in the side-side direction respectively with corresponding parameter choices. We choose the mass of the TMD m_1 to be 20000 kg because it is about 2% of the total structural mass of the turbine, which is a mass percentage normally used in civil structures (see Stewart & Lackner, 2013). The spring and damping constants of the TMDs are chosen to be 51320.72 N/m and 5427.46 N·s/m respectively in the fore-aft direction, and to be 51136.47 N/m and 5220.53 N·s/m respectively in the side-side direction. The parameters of tower part in Σ_d (3.48) - (3.49) can be obtained directly or through simple computations from the distributed properties of the NREL 5-MW monopile wind turbine tower, which are available in the table of page 12 in J. Jonkman (2006). The height l of the tower is 107.6 m. The mass of the RNA is 35005 kg whiles its moment of inertia is 4.5050443961×10^7 kg·m^2 in the side-side plane and is 2.4940615741×10^7 kg·m^2 in the fore-aft plane. The junction between the tower and monopile is not continuous and we smooth it by setting a 1-meter smooth transition region at the position $x \in [29.5\text{m}, 30.5\text{m}]$ (half from monopile region and the other half from the tower region) because our mathematical model Σ (3.1)-(3.5) requires that mass density function $\rho \in C^4(0,l)$ and flexural rigidity function $EI \in C^4(0,l)$. When $x \leq 29.5$ m, i.e, at the monopile region, $\rho = 9517.14$ kg/m; when $x > 30.5$ m, i.e., at the tower region, we use a 2nd-order polynomial to fit the discrete density data of the NREL 5-MW wind turbine tower by the least squares method. Then we fit the transitional region $x \in [29.5\text{m}, 30.5\text{m}]$ with a 9th-order polynomial to make $\rho \in C^4(0,l)$ for the whole monopile wind turbine tower. The flexural rigidity function EI is fitted in the same way. The fitted curves of ρ and EI are shown in Figure 4.

We use the same loading data for our model Σ_d (3.48) - (3.49) (i.e. its force F_e and torque T_e inputs) and the FAST-SC code, which is generated by TurbSim using IEC von Karman turbulence model with mean wind speed of 10 m/s and turbulence intensity of 15%. We compare the whole tower deflections and tower-top displacements of the NREL 5-MW baseline monopile wind turbine

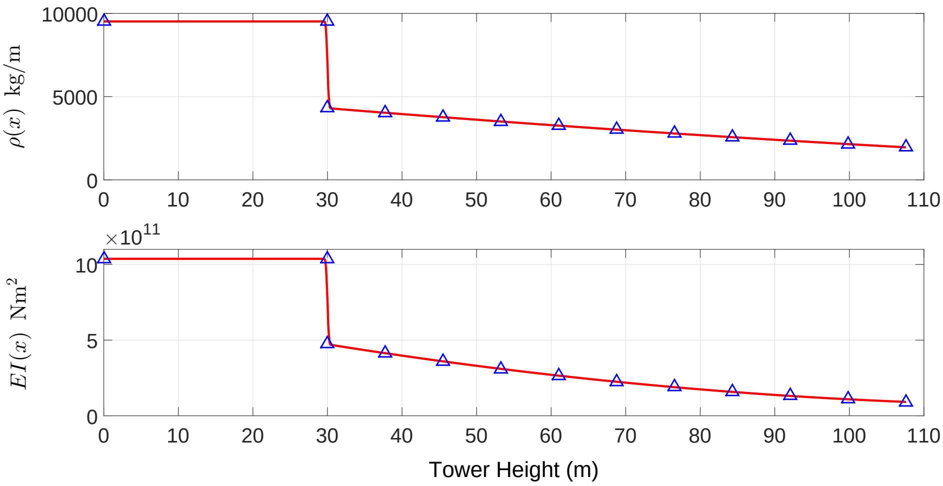

Figure 4. Comparisons between the distributed properties of mass density and flexural rigidity of the NREL 5-MW wind turbine tower and their corresponding fitted functions $\rho(x)$ and $EI(x)$. The blue triangles represent distributed tower properties given in the table of page 12 of J. Jonkman (2006) while the red solid lines are their corresponding fitted functions.

tower, computed from Σ_d (3.48) - (3.49) and FAST-SC simulations respectively, as shown in Figures 5 - 8. These figures clearly indicate that the dynamic outputs of Σ_d (3.48) - (3.49) are extremely close to the outputs of the FAST-SC simulations, which verifies our model. We have also conducted simulations for the case of a sole wind turbine tower using Σ_d (3.48) - (3.49) (excluding TMD) and FAST, which got similar agreements as Figures 5 - 8, thus omitted.

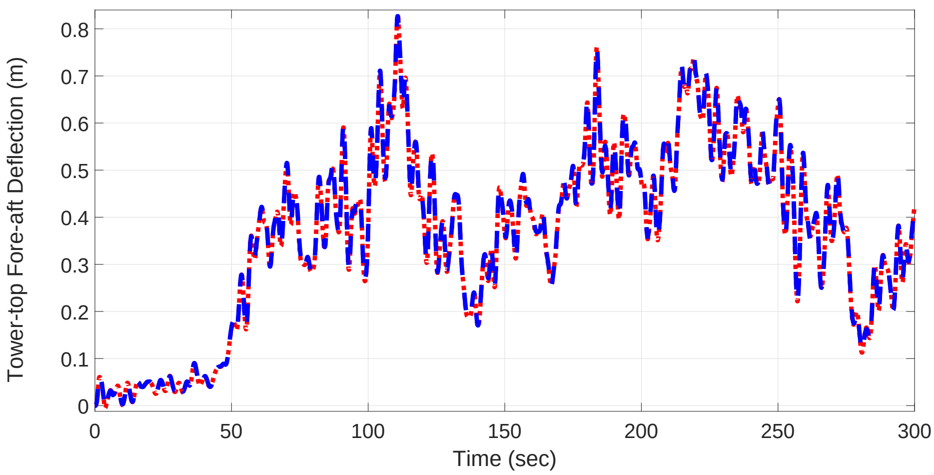

Figure 5. Time simulation (in seconds) of the fore-aft tower-top translational displacement (in meters) of the NREL 5-MW baseline monopile wind turbine tower stabilized by a fore-aft TMD under a wind input with mean speed of 10 m/s and turbulence intensity of 15%, obtained from Σ_d (3.48) - (3.49) (red dotted line) and FAST-SC (blue dash line) respectively.

Finally we compare the power spectral densities (PSDs) of the tower-top displacements for the case of a sole NREL 5MW wind turbine tower and the case of the tower stabilized by a TMD, computed from our model Σ_d (3.48) - (3.49) and FAST-SC simulations. As shown in Figures 9 and 10, the results obtained by our model agree perfectly with the ones obtained using the FASC-SC simulations in both cases with and without TMD.

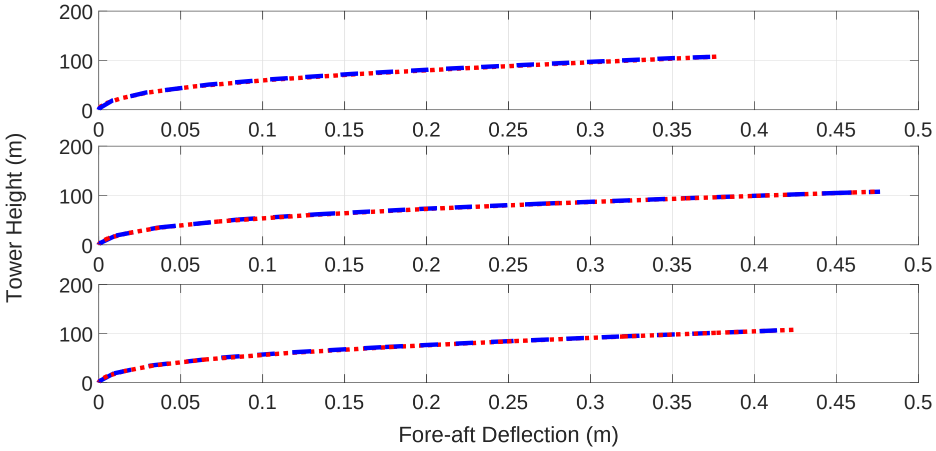

Figure 6. Simulation of the fore-aft translational deflections of the NREL 5-MW baseline monopile wind turbine tower stabilized by a fore-aft TMD under a wind input with mean speed of 10 m/s and turbulence intensity of 15%, obtained from Σ_d (3.48) - (3.49) (red dotted lines) and FAST-SC (blue dash lines) respectively. The upper, middle and lower diagrams show results at 100 s, 200 s and 300 s, respectively. The horizontal axis denotes the translational tower deflections (in meters) with positive value meaning "right" and negative value meaning "left", while the vertical axis describes the height of the tower (in meters).

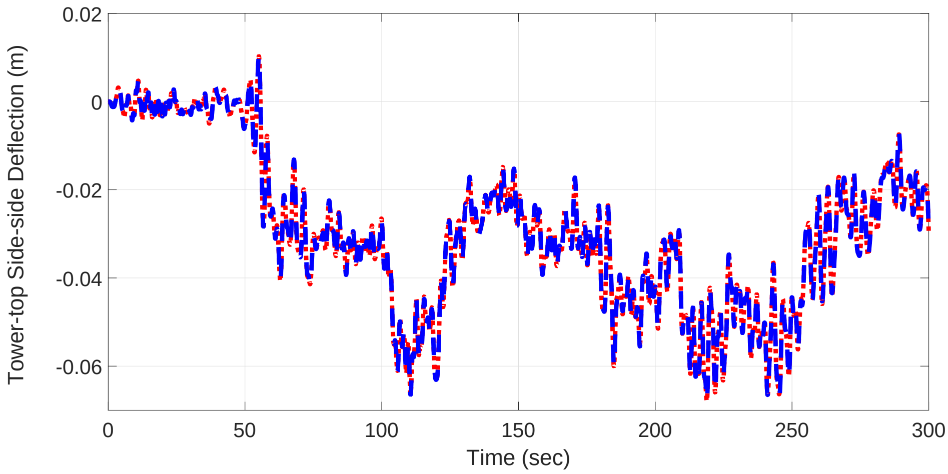

Figure 7. Time simulation (in seconds) of the side-side tower-top translational displacement (in meters) of the NREL 5-MW baseline monopile wind turbine tower stabilized by a side-side TMD under a wind input with mean speed of 10 m/s and turbulence intensity of 15%, obtained from Σ_d (3.48) - (3.49) (red dotted line) and FAST-SC (blue dash line) respectively.

4. Optimization of TMDs for load reduction of a monopile wind turbine tower

In this section, we employ $\mathcal{H}_2$ optimization to design optimal TMD for the monopile wind turbine tower - TMD model Σ_d (3.48) - (3.49). Recall that Σ_d can be used to represent the dynamics of the tower and TMD in the fore-aft direction and in the side-side direction respectively with corresponding parameter choices. We consider external force and torque $[F_e, T_e]^T$ as input (excitation sources) and the translational displacement $w(l, \cdot)$ of the tower top as output. As mentioned earlier, the largest deflection occurs at the tower top when the first mode is excited, which is the dominant mode of monopile wind turbine towers. Thus, to achieve optimal suppression of the vibrations of the wind turbine tower, we can choose optimal TMD parameters to minimize the $\mathcal{H}_2$-norm of the transfer function matrix $\mathbf{H}$ of Σ_d (3.48) - (3.49) with force and torque inputs and tower-top displacement output, as $\mathcal{H}_2$-norm serves to minimize the output variance under stochastic excitation

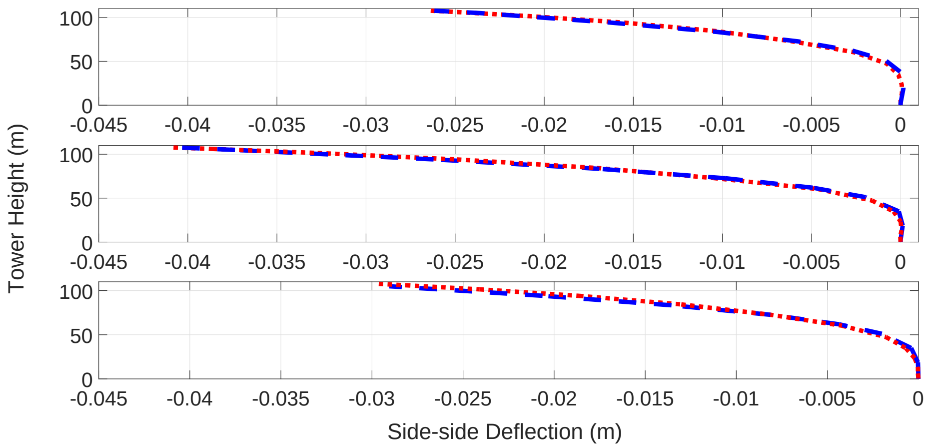

Figure 8. Simulation of the side-side translational deflections of the NREL 5-MW baseline monopile wind turbine tower stabilized by a side-side TMD under a wind input with mean speed of 10 m/s and turbulence intensity of 15%, obtained from Σ_d (3.48) - (3.49) (red dotted lines) and FAST-SC (blue dash lines) respectively. The upper, middle and lower diagrams show results at 100 s, 200 s and 300 s, respectively. The horizontal axis denotes the translational tower deflections (in meters) with positive value meaning "right" and negative value meaning "left", while the vertical axis describes the height of the tower (in meters).

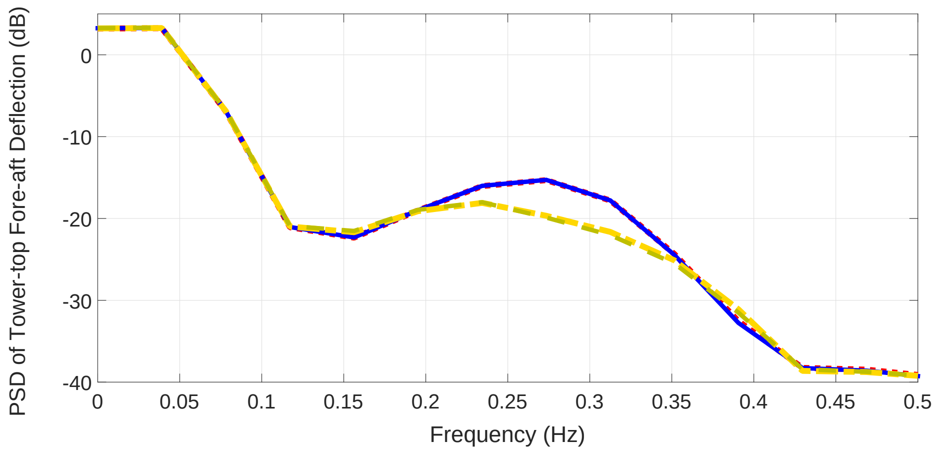

Figure 9. Power spectral density (PSD) of tower-top fore-aft translational displacement of the NREL 5-MW baseline monopile wind turbine tower under a wind input with mean speed of 10 m/s and turbulence intensity of 15%, obtained from Σ_d (3.48) - (3.49) (red dotted and yellow dash-dotted lines denoting cases of sole tower and tower stabilized by a fore-aft TMD, respectively) and FAST-SC (blue solid and green dash lines denoting cases of sole tower and tower stabilized by a fore-aft TMD, respectively).

(see Zuo & Nayfeh, 2002). Here we use the frequency-limited version of the $\mathcal{H}_2$-norm (4.50)

$$\|\mathbf{H}\|_{\mathcal{H}_{2,[\omega_1,\omega_2]}} = \frac{1}{\sqrt{2\pi}}\Big(\int_{-\omega_2}^{-\omega_1} trace\left[\mathbf{H}^*\left(j\nu\right)\mathbf{H}\left(j\nu\right)\right]d\nu + \int_{\omega_1}^{\omega_2} trace\left[\mathbf{H}^*\left(j\nu\right)\mathbf{H}\left(j\nu\right)\right]d\nu\Big)^{\frac{1}{2}}, \quad (4.50)$$

where $\mathbf{H}(s) = \mathbf{C}\left(s\mathbf{I}-\mathbf{A}\right)^{-1}\mathbf{B}$, $\omega_2 > \omega_1 \in \mathbb{R}^+$, and the superscript $*$ denotes complex conjugate transpose. $\mathbf{A}$, $\mathbf{B}$ and $\mathbf{C}$ are as in (3.48)-(3.49). This means to compute the $\mathcal{H}_2$-norm over a limited frequency range around the first modal frequency because the first bending mode dominates the dynamic response of monopile wind turbine towers.

To determine the frequency interval $[\omega_1, \omega_2]$, we need the first modal frequency of the monopile wind turbine tower, which is the smallest absolute value of the imaginary parts of eigenvalues of $\mathbf{A}$ in Σ_d (3.48) - (3.49) excluding TMD. Through simple computations, we get that the first tower fore-aft and side-side modal frequencies are 0.290 Hz (1.822 rad/s) and 0.287 Hz (1.806 rad/s) respectively, while they are both 0.28Hz in the FAST (see Passon et al., 2007). Here we use frequency

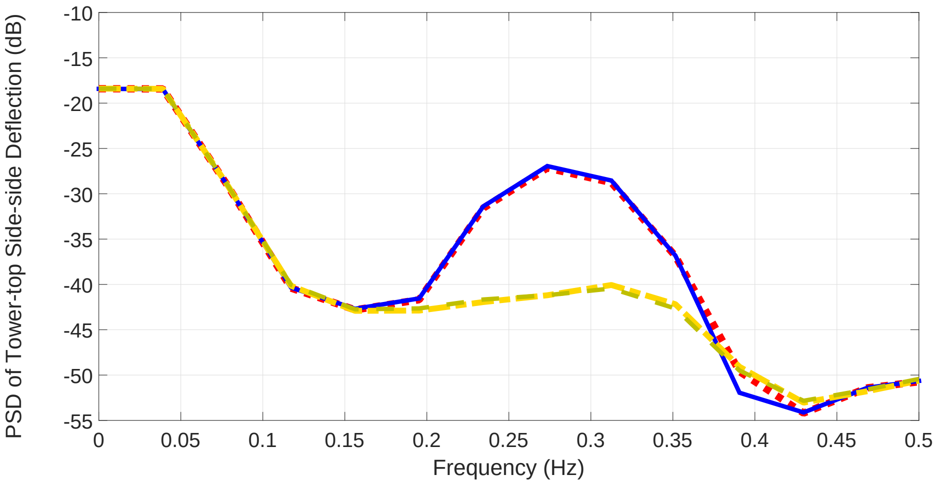

Figure 10. Power spectral density (PSD) of tower-top side-side translational displacement of the NREL 5-MW baseline monopile wind turbine tower under a wind input with mean speed of 10 m/s and turbulence intensity of 15%, obtained from Σ_d (3.48) - (3.49) (red dotted and yellow dash-dotted lines denoting cases of sole tower and tower stabilized by a side-side TMD, respectively) and FAST-SC (blue solid and green dash lines denoting cases of sole tower and tower stabilized by a side-side TMD, respectively).

Table 1. Values of the $\mathcal{H}_2$-norm (4.50) of Σ_d with N increasing from 9 to 17.

N	9	10	11	12	13	14	15	16	17
$\mathcal{H}_2$-norm ($\times 10^{-6}$)	1.891	1.890	1.893	1.893	1.892	1.895	1.894	1.895	1.893

intervals [1.458 rad/s, 2.186 rad/s] with the central frequency at 1.822 rad/s for the optimization of the fore-aft TMD and [1.445 rad/s, 2.167 rad/s] with the central frequency at 1.806 rad/s for the optimization of the side-side TMD, which can also be obtained through the PSD Figures 9 and 10.

We employ *fmincon* function of MATLAB to minimize the frequency-limited $\mathcal{H}_2$-norm (4.50) with spring and damping constants of TMD as design variables. All the other parameters of Σ_d are as in Section 3.3. Recall that the mass of the TMD is chosen to be 20000 kg (about 2% of the total structural mass of the turbine). We get that the optimal spring and damping constants are 61514.97 N/m and 7518.93 N·s/m respectively in the fore-aft TMD, and are 60565.20 N/m and 7405.66 N·s/m respectively in the side-side TMD. It is noticeable that the natural frequencies of the fore-aft TMD (0.279 Hz) and side-side TMD (0.277 Hz) are both approximately equal to their corresponding first modal frequencies of the monopile wind turbine tower.

We mention that the discretization resolution (i.e., the number of collocation points) we used for conducting model verification in Section 3.3 as well as for optimizing TMD above is $N = 13$. Ideally, the value of N should be independent of the $\mathcal{H}_2$-norm (4.50), which implies that as N increases, the $\mathcal{H}_2$-norm of $\mathbf{H}$ should converge to a small range. Table 1 lists its values in the fore-aft direction with N increasing from 9 to 17. Clearly, it converges to a small narrow range between between 1.890×10^{-6} and 1.895×10^{-6}, which means that the relative error is less than 0.27%. The result for the $\mathcal{H}_2$-norm of $\mathbf{H}$ in the side-side direction is similar and thus omitted.

5. Simulation tests

We now test our optimal TMD designs based on the simulations of the NREL 5-MW baseline monopile wind turbine model within FAST-SC. First we measure and compare the average damage equivalent loads (DEQL) at the monopile base of the NREL 5-MW baseline monopile wind turbine model for the cases with and without TMD(s) under wind and wave excitations. Note that the monopile base of the monopile wind turbine tower has the largest bending moment (maximum

Table 2. Simulation results of the average damage equivalent loads (DEQL) at the monopile base of the NREL 5-MW baseline monopile wind turbine model for the cases of sole tower (no TMD), tower stabilized by a fore-aft TMD, tower stabilized by a side-side TMD, tower stabilized by both (the fore-aft and side-side) TMDs. The data outside the brackets are obtained using our optimal TMDs while the ones in the brackets are obtained using TMDs designed in Stewart and Lackner (2013). "Load A" denotes a wind input with mean speed of 10 m/s and turbulence intensity of 15%, and a wave input with significant wave height of 2 m. It's generated twice by two different random seeds with DEQL being averaged values under both excitations. "Load B" denotes a wind input with mean speed of 18 m/s and turbulence intensity of 15%, and a wave input with significant wave height of 3.5 m. It's generated twice by two different random seeds with DEQL being averaged values under both excitations as well.

	No TMD	Fore-aft TMD	Side-side TMD	Both TMDs
Fore-aft DEQL (kN·m), load A	15275	12628 (12442)	15507 (15496)	12948 (12737)
Reduction from no TMD case	N/A	17.3% (18.5%)	-1.52% (-1.45%)	15.2% (16.6%)
Side-side DEQL (kN·m), load A	3871	3831 (3752)	1214 (1205)	1182 (1150)
Reduction from no TMD case	N/A	1.03% (3.07%)	68.6% (68.9%)	69.5% (70.3%)
Fore-aft DEQL (kN·m), load B	28011	22272 (22368)	28402 (28396)	22140 (22448)
Reduction from no TMD case	N/A	20.5% (20.1%)	-1.40% (-1.37%)	21.0% (19.9%)
Side-side DEQL (kN·m), load B	7263	7090 (6806)	2271 (2249)	2199 (1946)
Reduction from no TMD case	N/A	2.38% (6.29%)	68.7% (69.0%)	69.7% (73.2%)

stress) (see Chen, Huang, Bretel, & Hou, 2013). We verify our results against Stewart and Lackner (2013). As obtained in Section 4, our optimal spring and damping constants are 61514.97 N/m and 7518.93 N·s/m respectively in the fore-aft TMD, and are 60565.20 N/m and 7405.66 N·s/m respectively in the side-side TMD. In Stewart and Lackner (2013) the optimal spring and damping constants of the TMDs in the fore-aft and the side-side directions are the same, i.e., 54274 N/m and 7414 N·s/m respectively. The mass of the TMD is chosen to be 20000 kg in all the cases.

The wind inputs are generated by TurbSim using IEC von Karman turbulence model with turbulence intensity of 15%. The power law exponent is set to be 0.14. The waves are irregularly (stochastically) generated based on the JONSWAP/Pierson-Moskowitz frequency spectrum. We use Wheeler model for stretching incident wave kinematics to instantaneous free surface. The peak spectral period of incident waves is set to be 12.4 seconds. Here we assume that the wave and wind are both in the fore-aft direction. Four types of wind and wave inputs are generated for simulations. Two inputs are generated by different random seeds based on the same mean wind speed of 10 m/s (below the rated value 11.4 m/s, in control region 2) and same significant wave height of 2 m. We take averages for the DEQL simulation results with these two types of inputs. The other two inputs are also generated by different random seeds based on the same mean wind speed of 18 m/s (above-rated, in control region 3) and same significant wave height of 3.5 m. We take averages for the DEQL simulation results with these two types of inputs as well. We simulate three cases: the sole tower case (i.e., without TMDs), the case using the optimal TMDs obtained in Section 4, and the case using TMDs designed in Stewart and Lackner (2013). For the cases with TMDs, we consider three kinds of TMD configurations: only the fore-aft TMD, only the side-side TMD, and both (the fore-aft and side-side) TMDs.

We use the MLife code provided by NREL to compute DEQL, which employs a rainflow counting algorithm to post-process results from wind turbine simulations for this computation. The frequency of DEQL is set to be 1 Hz. The Wohler exponent is set to be 3. For details about MLife, we refer to Hayman (2012). Table 2 lists the DEQL at the monopile base of the NREL 5-MW baseline monopile wind turbine model and load reduction ratios with TMDs designed by us and Stewart and Lackner (2013) under the wind and wave inputs mentioned above. It is noticeable from Table 2 that we get similar vibration control results as Stewart and Lackner (2013). But our control design model can simulate the dynamics of the wind turbine tower very accurately as shown in Figures 5 - 8.

Finally we compare the PSDs of the tower-top translational deflections of the sole tower and of the tower stabilized by our optimal fore-aft and side-side TMDs based on FAST-SC simulations under a wind input with mean speed of 18 m/s and turbulence intensity of 15%, and a wave input with significant wave height of 3.5 m. As shown in Figures 11 and 12, our optimal TMDs have achieved substantial vibration reductions.

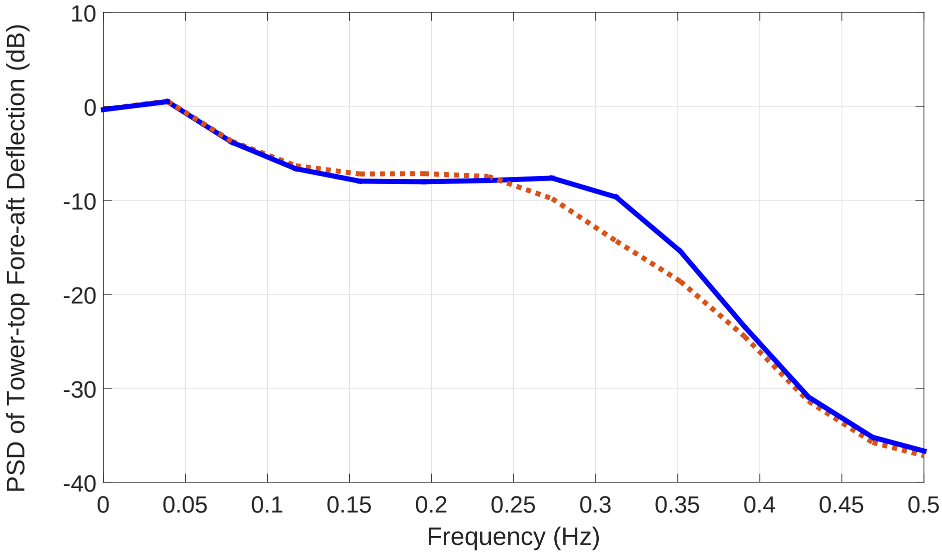

Figure 11. Power spectral density (PSD) of the tower-top fore-aft translational deflections of the NREL 5-MW monopile wind turbine tower based on FAST-SC simulations under a wind input with mean speed of 18 m/s and turbulence intensity of 15%, and a wave input with significant wave height of 3.5 m. Blue solid and red dotted lines denote cases of sole tower and tower stabilized by optimal fore-aft and side-side TMDs designed by us, respectively.

6. Conclusions

We have successfully used a TMD system to suppress the vibration of monopile wind turbine tower. There are a TMD in the fore-aft direction and a TMD in the side-side direction respectively, which share the same mass component. The mass component of the TMD is put on the floor of the nacelle through wheels/racks (reducing friction). The spring and damper components of each TMD are connected at one end to the nacelle of the wind turbine and linked at the other end to its mass component in parallel. Similar TMD systems have been used in the John Hancock Tower in Boston and the Citicorp Center in Manhattan which reduced worst-case wind-induced motion up to 50%. It can also be hanged above the floor through cables like the case of Taipei 101 skyscraper in Taipei.

We made infinite-dimensional model Σ (3.1)-(3.5) of the monopile wind turbine tower-TMD system applicable to our optimization scheme by discretizing its PDE formulation along the tower's span to derive its finite-dimensional version Σ_d (3.48) - (3.49) using the spectral element method. Σ_d can be used to represent the dynamics of the tower and TMD in the fore-aft direction and in the side-side direction respectively with corresponding parameter choices. We verified Σ_d against the NREL 5-MW wind turbine model. Then we derived the transfer function matrix of Σ_d with force and torque acting on the RNA as the input and tower-top translational displacement as the output, based on which we performed $\mathcal{H}_2$ optimization. Since the motion of the monopile wind

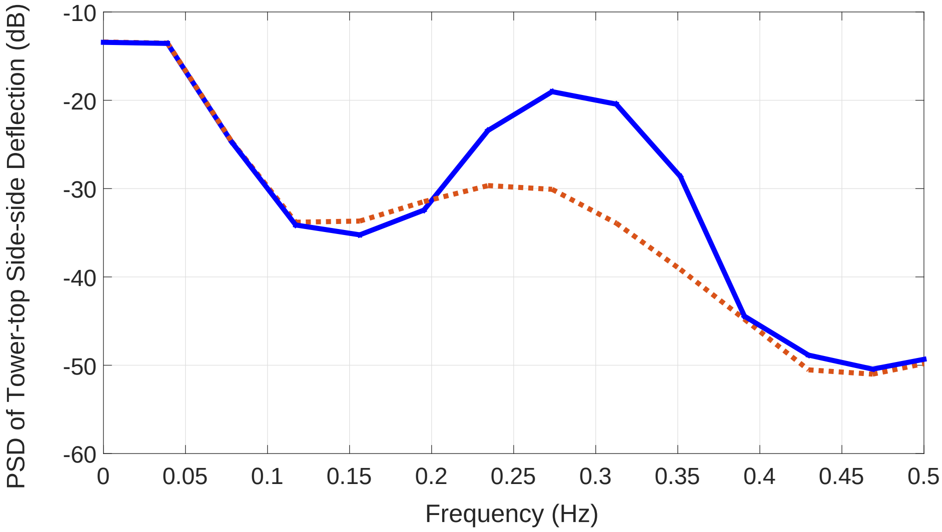

Figure 12. Power spectral density (PSD) of the tower-top side-side translational deflections of the NREL 5-MW monopile wind turbine tower based on FAST-SC simulations under a wind input with mean speed of 18 m/s and turbulence intensity of 15%, and a wave input with significant wave height of 3.5 m. Blue solid and red dotted lines denote cases of sole tower and tower stabilized by optimal fore-aft and side-side TMDs designed by us, respectively.

turbine tower is dominated by its first mode, we used frequency-limited $\mathcal{H}_2$ optimization to save computation time, based on which we obtained optimal fore-aft and side-side TMDs for the NREL 5-MW monopile wind turbine tower.

We verified the performance of our optimal TMD(s) against Stewart and Lackner (2013), which got similar results. But our model is more realistic, which contains many vibration modes and thus can simulate the dynamics of the tower more precisely than a rigid inverted pendulum model with only one mode. Besides, our model can also be easily extended to floating wind turbine towers or a more general flexible structure, which might have more than one modes dominating the vibration dynamics. The extended model can allow the design of multiple TMDs to suppress more vibration modes. Furthermore, all parameters required by our model can be obtained directly or through simple computations from parameters provided by manufacturers, which does not need system identification which is very difficult to conduct on a real wind turbine tower. In addition the $\mathcal{H}_2$ optimization scheme employed by our design is more systematic than optimization through simulation under specific loading excitation. Furthermore our work has successfully demonstrated how to optimally tune a TMD to reduce vibrations of flexible structures described by partial differential equations.

We would like to mention that the control design method of this paper can be extended to vibration reductions of flexible structures with more dominant modes, where multiple TMDs will be employed with each TMD being placed at the antinode of the mode shape of a dominant mode. We use an non-uniform SCOLE beam as an illustrative example and consider the trade-off between effectiveness and robustness of multiple TMDs under harmonic and random excitations. The results will be reported elsewhere. Here we provide a brief glimpse. The SCOLE beam used for analysis has the following parameters: $l = 1$, $\rho(x) = EI(x) = -0.1x + 0.2$, $m = 0.05$, $J = 0.1$. It has two dominant vibration modes with modal frequencies $\omega_1 = 1.1203\,\mathrm{rad/s}$ and $\omega_2 = 4.6184\,\mathrm{rad/s}$. Their corresponding mode shapes are shown in Figure 13. The antinodes of the first and second mode shapes are located at $x = 1$ (beam top) and $x = 0.95$, respectively. Figure 14 summarizes the standard deviations (STDs) of the transverse displacements of the SCOLE beam system at $x = 1$ and $x = 0.95$ for the uncontrolled case (black solid lines) and the case stabilized by two TMDs optimized by our scheme with each TMD being tuned for a dominant mode (blue dotted lines), under harmonic excitations with the excitation frequencies varying from ω_1 to ω_2. It's clear from this figure that the two TMDs have effectively damped the vibrations caused by the two dominant modes.

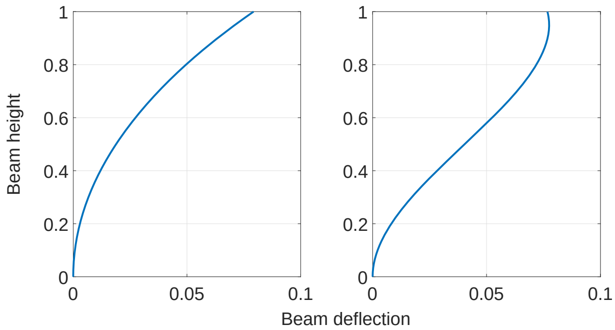

Figure 13. Mode shapes of the first two modes of a SCOLE beam. The left-hand diagram shows the mode shape of the first mode while the right-hand one is the mode shape of the second mode.

References

Boyd, J. P. (2001). *Chebyshev and fourier spectral methods* (second ed.). New York: Dover Publications,Inc.

BTM Consult. (2011). *International wind energy development: world market update 2010.* Retrieved from `http://www.navigant.com/ /media/WWW/site/downloads/energy/world_market_update_2010.ashx`

Chen, D., Huang, K., Bretel, V., & Hou, L. (2013). Comparison of structural properties between monopile and tripod offshore wind-turbine support structures. *Advances in Mechanical Engineering*.

Darrow, P. J. (2010, January). *Wind turbine control design to reduce capital costs* (Tech. Rep.). National Renewable Energy Laboratory (NREL).

Hayman, G. J. (2012, October). *MLife theory manual for version 1.00* (Tech. Rep.). National Renewable Energy Laboratory (NREL).

Jonkman, J. (2006, June). *Manuscript document of NREL's baseline wind turbine aeroelastic model for use in various offshore analysis concept studies.* Retrieved from `http://www.ieawind.org/AnnexXXIIISecure/Subtask_2S_docs/OC3Files/BaselineTurbine/NRELOffshrBsline5MW.pdf`

Jonkman, J., Butterfield, S., Musial, W., & Scott, G. (2009, February). *Definition of a 5-MW reference wind turbine for offshore system development* (Tech. Rep.). National Renewable Energy Laboratory (NREL).

Jonkman, J., Marshall, L., & Buhl, J. (2005, August). *FAST user's guide* (Tech. Rep.). National Renewable Energy Laboratory (NREL).

Jonkman, J. M., Robertson, A. N., & Hayman, G. J. (to appear). *HydroDyn users guide and theory manual* (Tech. Rep.). National Renewable Energy Laboratory (NREL).

Lackner, M. A., & Rotea, M. A. (2011, April). Passive structural control of offshore wind turbines. *Wind Energy*, *14*(3), 373-388.

Leithead, W. E., Dominguez, S., & Spruce, C. (2004, November). Analysis of tower/blade interaction in the cancellation of the tower fore-aft mode via control. In *European wind energy conference 2004*. London.

Littman, W., & Markus, L. (1988a). Exact boundary controllability of a hybrid system of elasticity. *Archive for Rational Mechanics and Analysis*, *103*, 193–235.

Littman, W., & Markus, L. (1988b). Stabilization of a hybrid system of elasticity by feedback boundary damping. *Annali di Matematica Pura ed Applicata*, *152*(1), 281–330.

NWTC. (2014a). *NWTC information portal (AeroDyn).* Retrieved from `https://nwtc.nrel.gov/AeroDyn`

NWTC. (2014b). *NWTC information portal (TurbSim).* Retrieved from `https://nwtc.nrel.gov/TurbSim`

Passon, P., Kuhn, M., Butterfield, S., Jonkman, J., Camp, T., & Larsen, T. J. (2007). OC3-benchmark exercise of aero-elastic offshore wind turbine codes. In *Journal of physics: Conference series* (Vol. 75).

Sadek, F., Mohraz, B., Taylor, A. W., & Chung, R. M. (1997). A method of estimating the parameters of

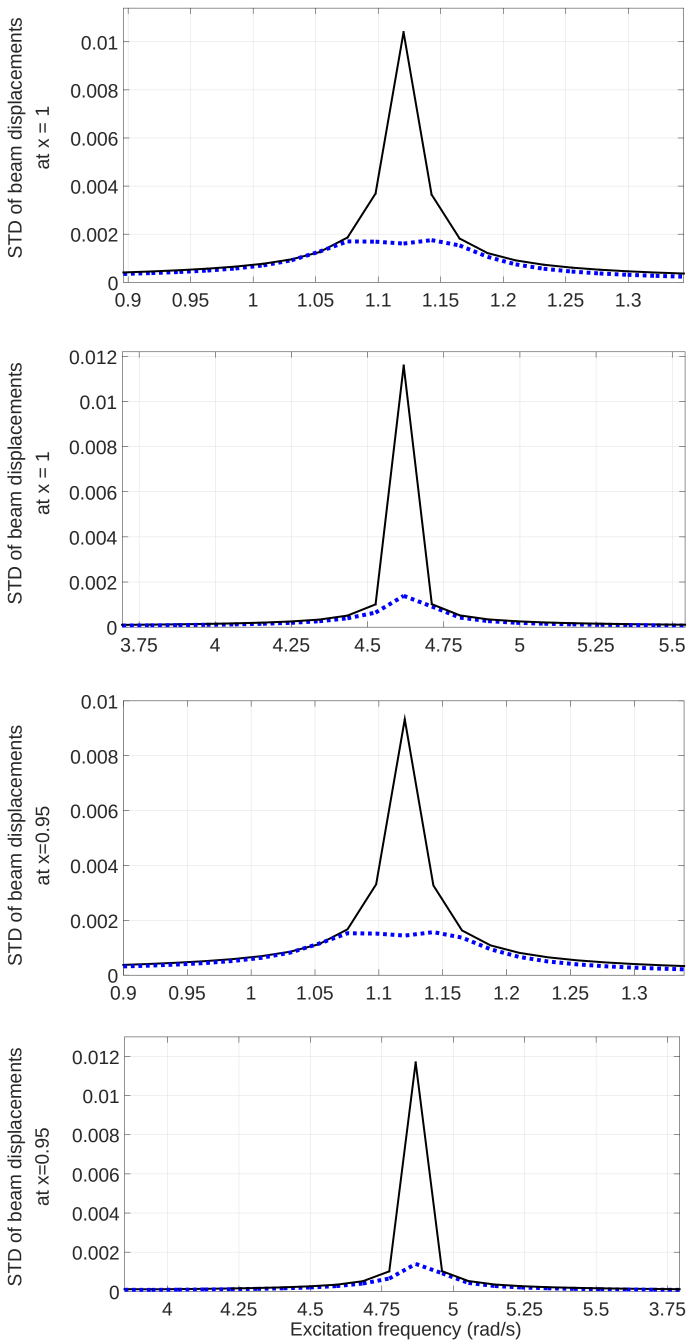

Figure 14. STD of the transverse displacements of a SCOEL beam at the $x = 1$ (beam top) and at $x = 0.95$ versus the excitation frequency. Black solid and blue dotted lines are for the uncontrolled case and the case stabilized by two optimal TMDs with each one being placed at the antinode of the mode shape of a dominant mode, respectively.

tuned mass dampers for seismic applications. *Earthquake Engineering and Structural Dynamics*, *26*, 617–635.

Soltani, M., Wisniewski, R., Brath, P., & Boyd, S. (2011, September). Load reduction of wind turbines using receding horizon control. In *Proceedings IEEE multi-conference on systems and control* (p. 852-857).

Soong, T. T., & Spencer, B. (2002, March). Supplemental energy dissipation: state-of-the-art and state-of-the-practice. *Engineering Structures*, *24*(3), 243-259.

Spencer, B., & Nagarajaiah, S. (2003, July). State of the art of structural control. *Journal of Structural Engineering*, *129*(7), 845-856.

Stewart, G., & Lackner, M. A. (2013, July). Offshore wind turbine load reduction employing optimal passive tuned mass damping systems. *IEEE Transactions on Control Systems Technology*, *21*(4), 1090–1104.

Teena, T. (2010). High demand for wind farm installation vessels. *Hansa International Maritime Journal*, *147*(8), 170–171.

The European Wind Energy Association [EWEA]. (2014). *Wind in power 2013 European statistics.* Retrieved from http://www.ewea.org/fileadmin/files/library/publications/statistics/EWEA_Annual_Statistics_2013.pdf

World Wind Energy Association [WWEA]. (2011). *World wind energy report 2010.* Retrieved from http://www.fondazionesvilupposostenibile.org/f/News/Rapporto+WWEA+2010+sull%27+eolico+nel+mondo.pdf

Zhang, Z., Neilsen, S. R. K., Blaabjerg, F., & Zhou, D. (2014). Dynamics and control of lateral tower vibrations in offshore wind turbines by means of active generator torque. *Energies*, *7*, 7746-7772.

Zhao, X., & Weiss, G. (2011a). Suppression of the vibrations of wind turbine towers. *IMA Journal of Mathematical Control and Information*, *28*, 377-389.

Zhao, X., & Weiss, G. (2011b). Well-posedness and controllability of a wind turbine tower model. *IMA Journal of Mathematical Control and Information*, *28*, 103–119.

Zhao, X., & Weiss, G. (2014). Stabilization of a wind turbine tower model in the plane of the turbine blades. *International Journal of Control*, *87*, 2027–2034.

Zhao, X., & Weiss, G. (2015, July). Strong stabilization of the scole model using a tuned mass damper. In *SIAM conference on control and its applications.* Paris, France.

Zuo, L., & Nayfeh, S. (2002). Design of passive mechanical systems via decentralized control techniques. In *43rd AIAA/ASME/ASCE/AHS/ASC Structures, Structural Dynamics, and Materials Conference, AIAA.*